Supporting Information for

Tuning the Selectivity of Benzylamine Photo-oxidation with Different Rhodium Modes Anchoring on $BiOIO_3$

Jiaping Liu,[‡a] Yan Wu,[‡a] Qingqing Chen,[‡a] Rui Yu,[a] Keqing Shi,[b] Tao Jing,[d] Zhujie Li,[b*] Zaizhu Lou,[c*] and Gang Wang[a*]

Figs and Tables

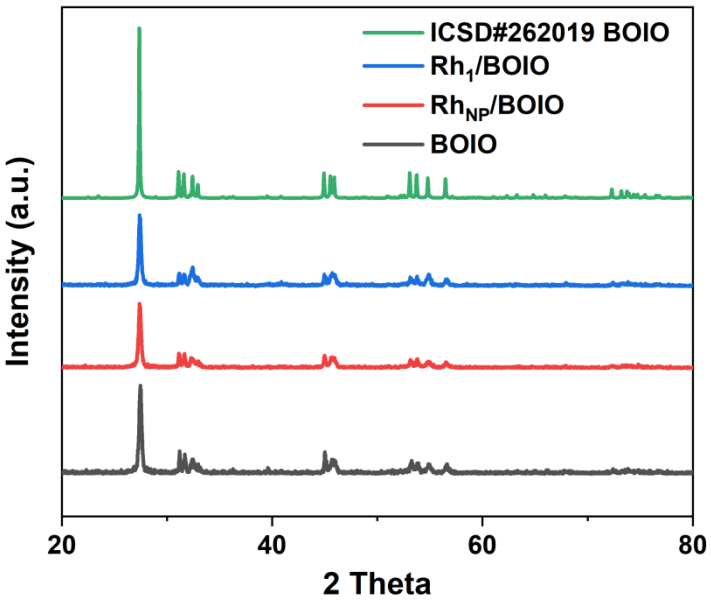

Fig. S1 XRD patterns of the Rh_1/BOIO, Rh_{NP}/BOIO, BOIO and the standard BOIO.

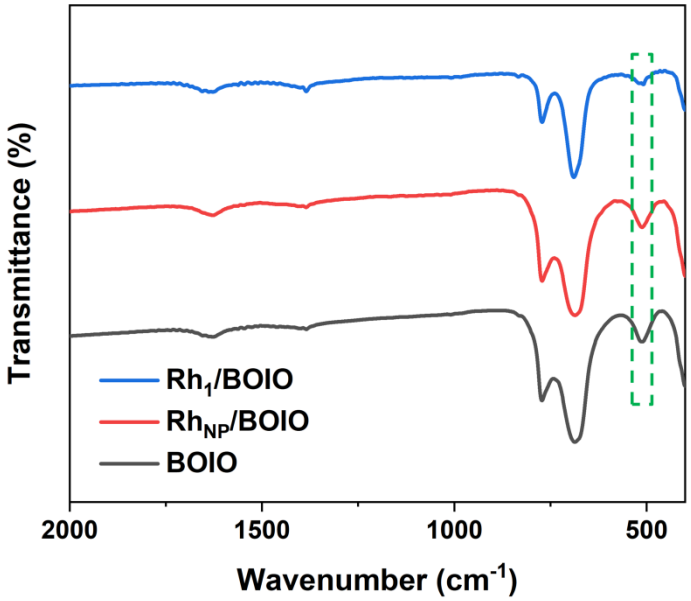

Fig. S2 The Fourier transforms infrared spectroscopy (FT-IR) of samples. The peak at around 514 cm^{-1} is the stretching vibration of Bi-O of BOIO (green box). In Rh_1/BOIO, the characteristic peak of Bi-O has been reduced, which could attribute to the formation of Rh-O bond.

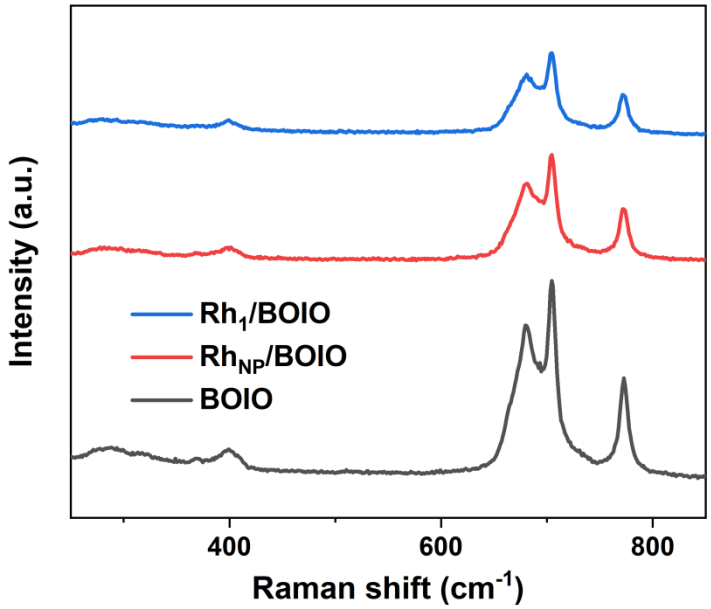

Fig. S3 The Raman spectra of Rh_1/BOIO, Rh_{NP}/BOIO and BOIO.

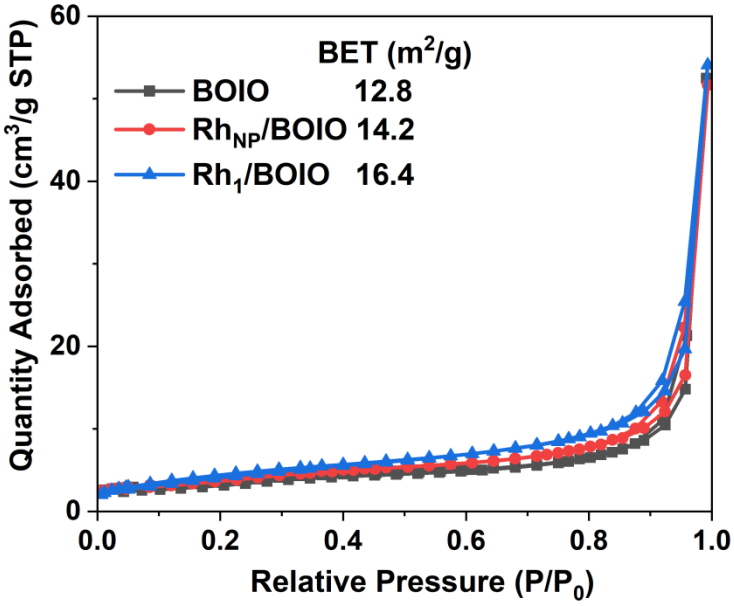

Fig. S4 Nitrogen adsorption and desorption isotherms of Rh_1/BOIO, Rh_{NP}/BOIO and BOIO.

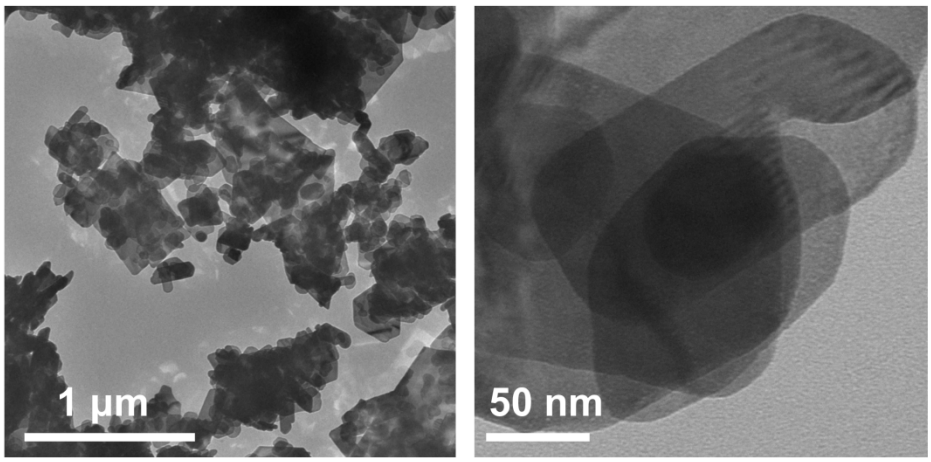

Fig. S5 TEM images of BOIO.

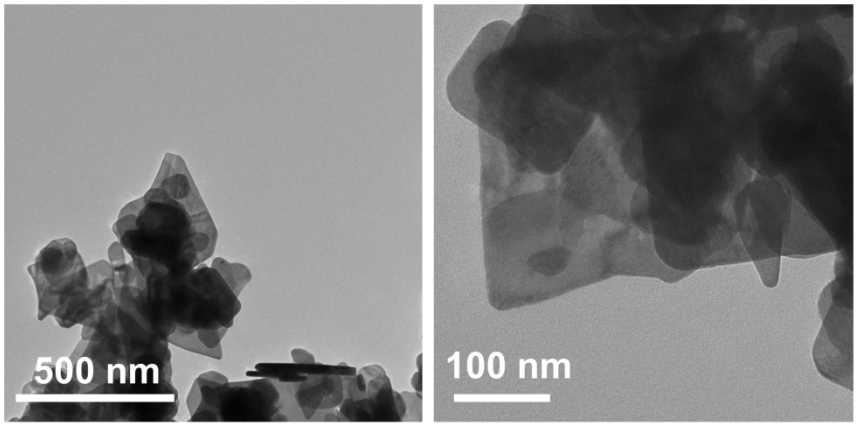

Fig. S6 TEM images of Rh_1/BOIO.

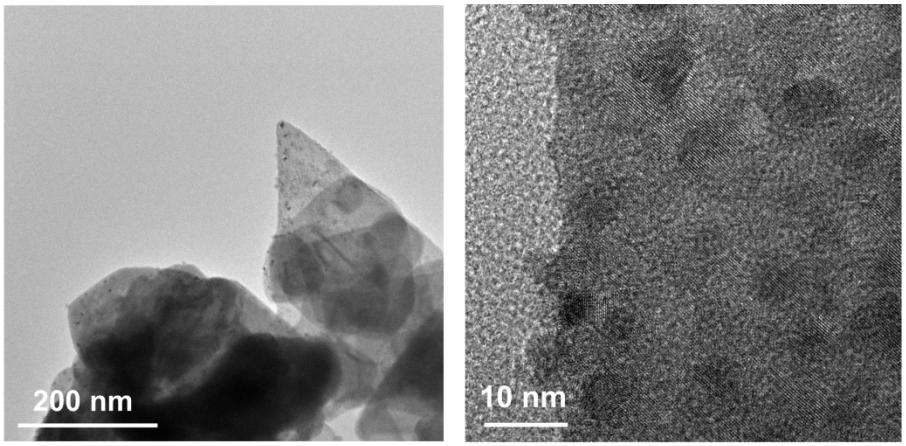

Fig. S7 TEM images of Rh_{NP}/BOIO.

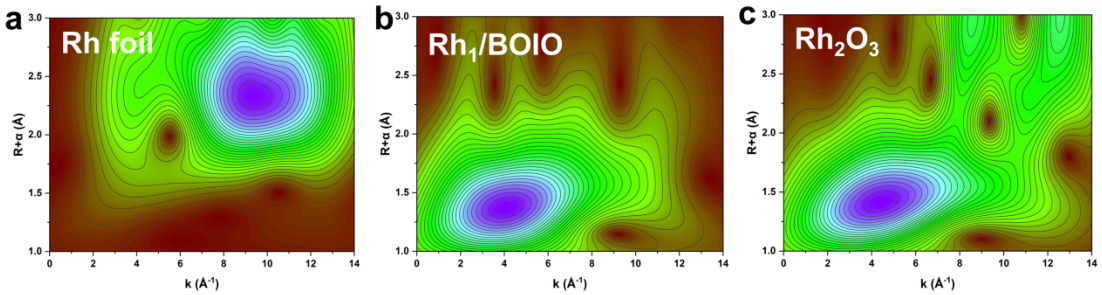

Fig. S8 WT plots of samples. (a) Rh foil, (b) Rh_1/BOIO and (c) Rh_2O_3.

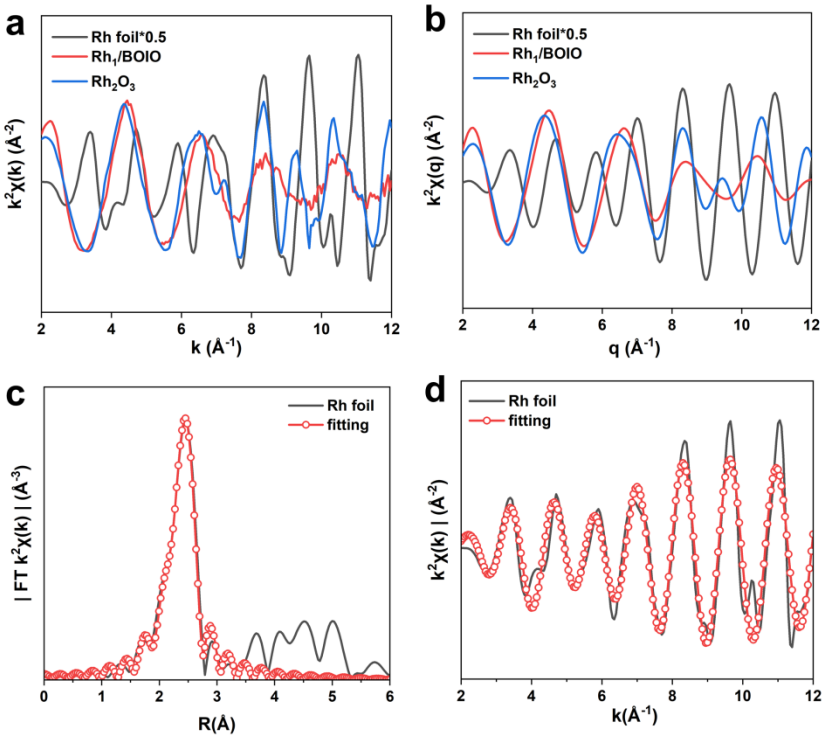

Fig. S9 (a) The k-space spectra of EXAFS of Rh foil, Rh_2O_3 and Rh_1/BOIO. (b) The q-space spectra of EXAFS of Rh foil, Rh_2O_3 and Rh_1/BOIO. (c) R-space fitting results of Rh foil. (d) k-space fitting results of Rh foil.

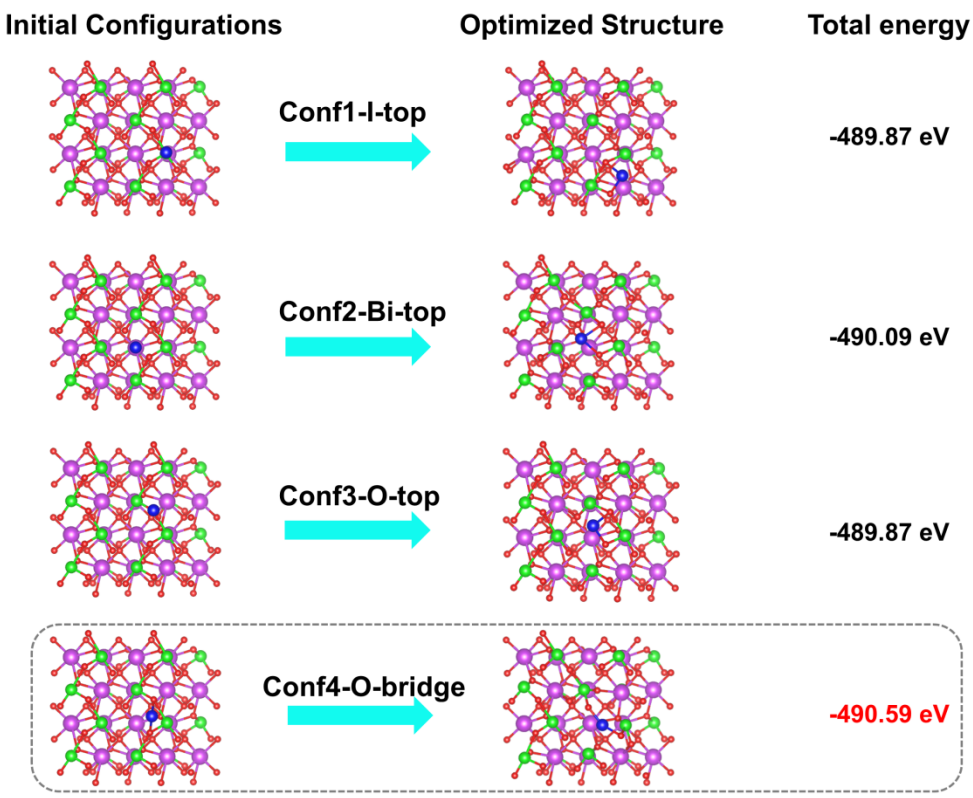

Fig. S10 The optimized structure of Rh_1/BOIO. These are four different initial configurations have been established, Conf1-I-top, Conf2-Bi-top, Conf3-O-top and Conf4-O-bridge. The most stable configuration of Conf4-O-bridge can be confirmed after structural optimization. purple ball: Bi, green ball: I, red ball: O, blue ball: Rh.

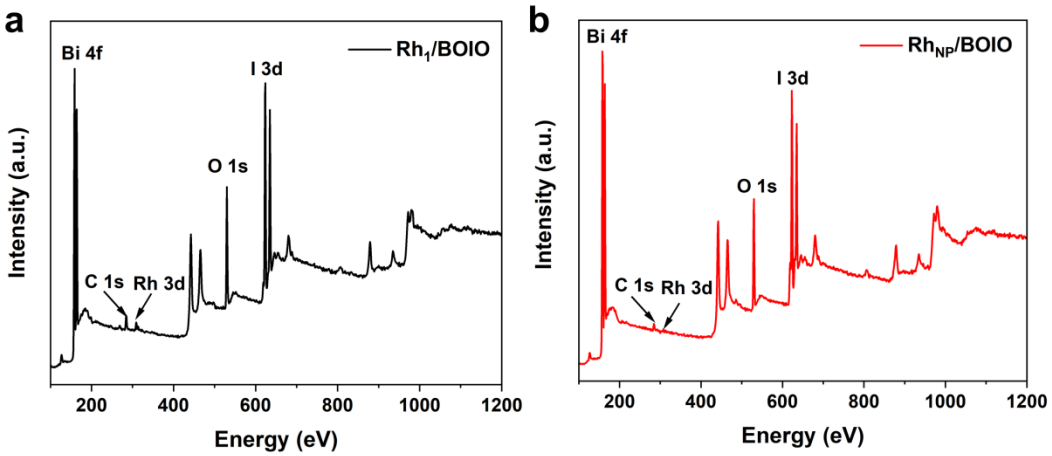

Fig. S11 XPS survey spectrum of the as-prepared (a) Rh_1/BOIO and (b) Rh_{NP}/BOIO.

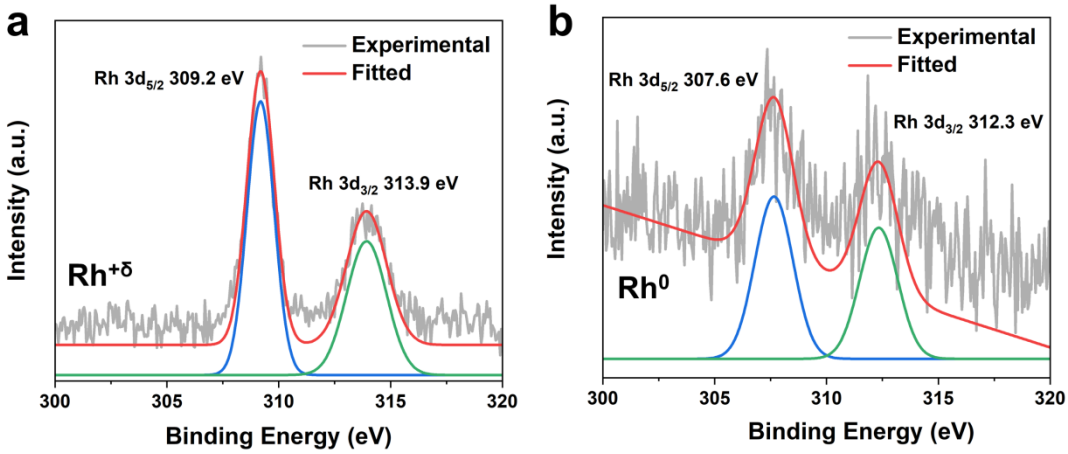

Fig. S12 XPS results of Rh 3d of (a) Rh_1/BOIO ($0<\delta<3$) and (b) Rh_{NP}/BOIO.

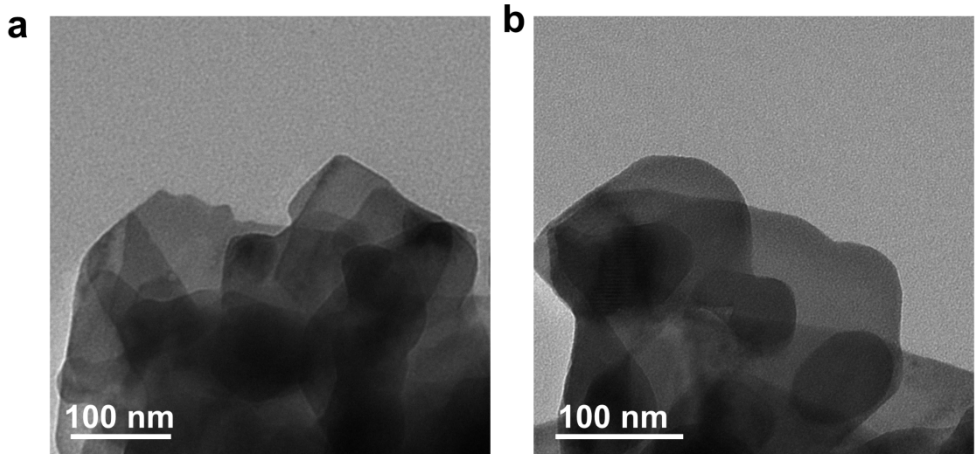

Fig. S13 TEM images of (a) Rh_1-0.34wt% and (b) Rh_1-1.04wt%. Rh_1-0.34wt% sample was obtained after photo-deposition process between 61 μL $RhCl_3•xH_2O$ solution (0.1 g mL^{-1}) and 0.3 g BOIO. 183μL $RhCl_3•xH_2O$ solution (0.1 g mL^{-1}) was mixed with 0.3 g BOIO to obtain Rh_1-0.34wt% sample after light irradiation.

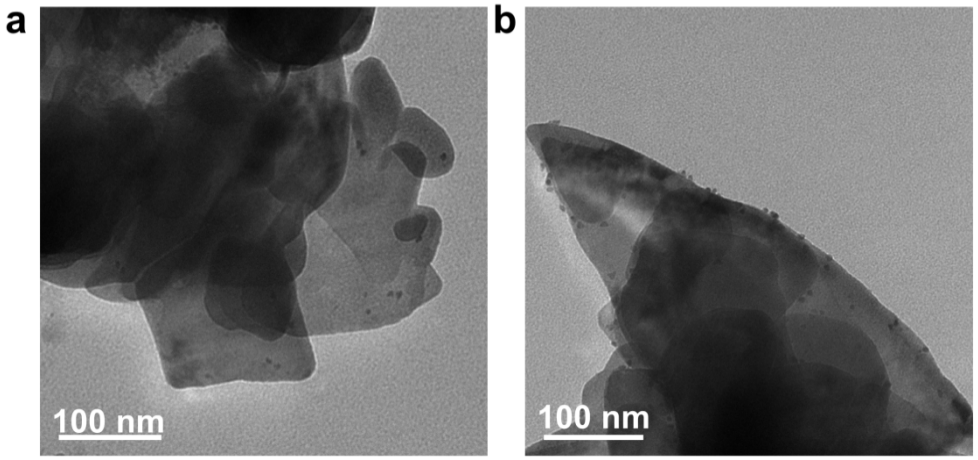

Fig. S14 TEM images of (a) Rh_{NP}-0.35wt% and (b) Rh_{NP}-1.04wt%. The samples were obtained via controlling the amount of as-prepared Rh_{NP}.

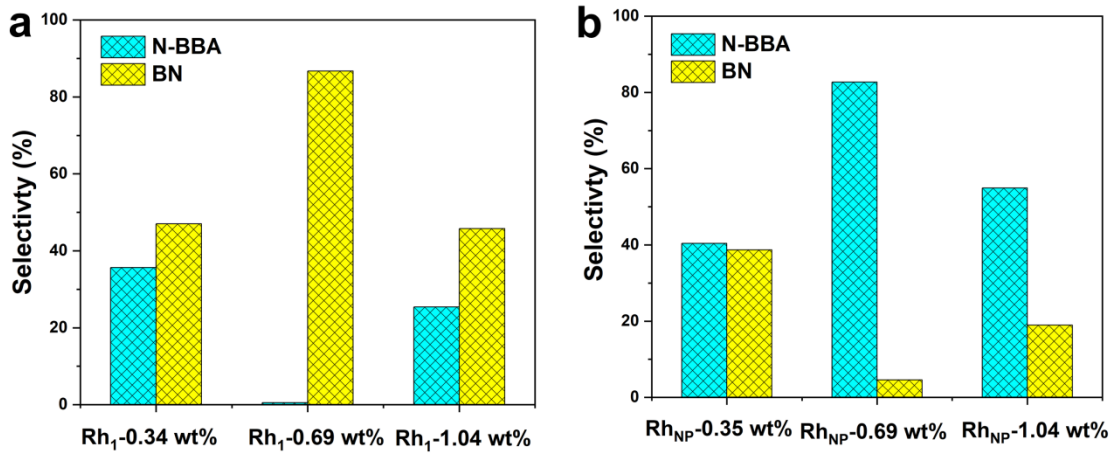

Fig. S15 (a) The selectively of N-BBA and BN over different Rh_1 amount on BOIO surface, Rh_1-0.69 wt% is the Rh_1/BOIO sample (b) The selectively of N-BBA and BN over different Rh_{NP} amount on BOIO surface, Rh_{NP}-0.69 wt% is the Rh_{NP}/BOIO sample. The optimized loading amounts of Rh species for Rh_1/BOIO and Rh_{NP}/BOIO have been confirmed.

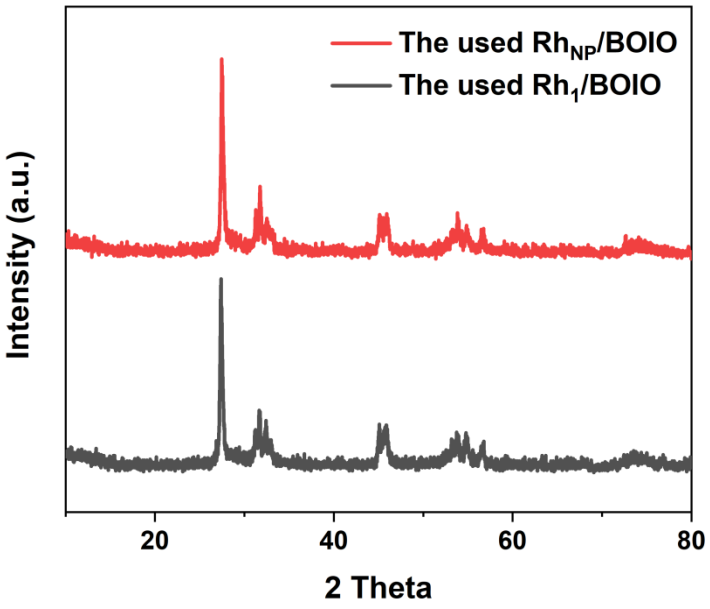

Fig S16. The XRD patterns of the used Rh_1/BOIO and Rh_{NP}/BOIO.

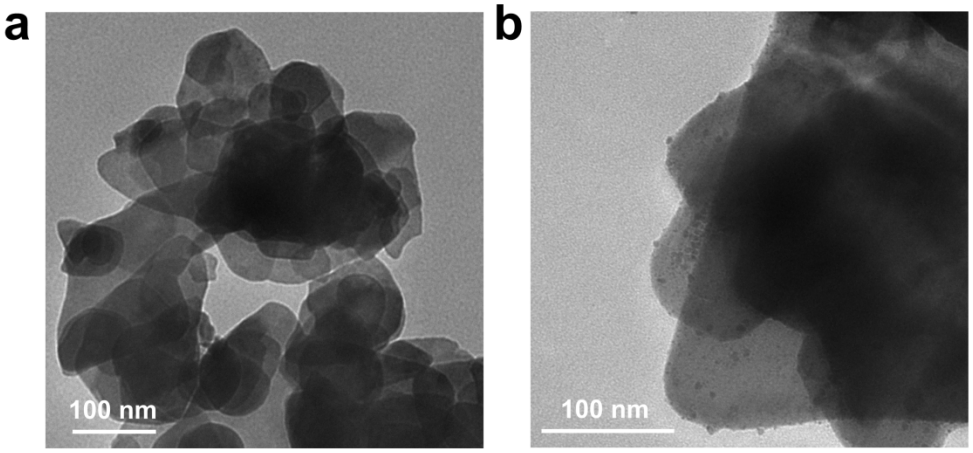

Fig S17. The TEM images of the used (a) Rh_1/BOIO and (b) Rh_{NP}/BOIO.

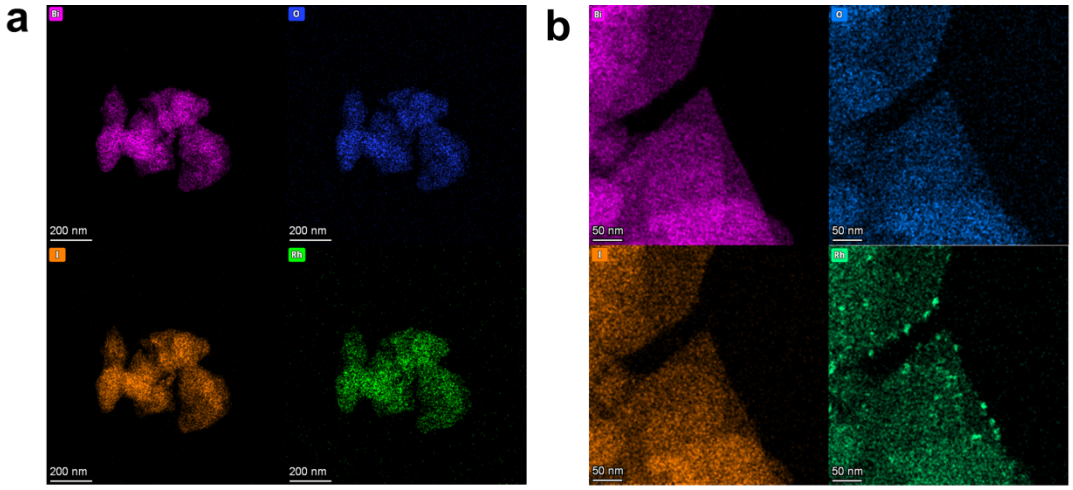

Fig S18. The elements mapping images of the used (a) Rh_1/BOIO and (b) Rh_{NP}/BOIO

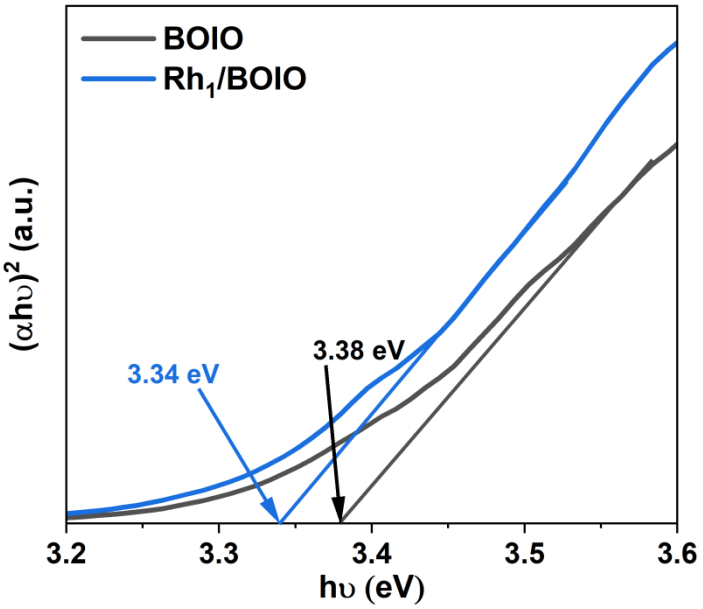

Fig S19. The obtained bandgap of samples via Kubelka–Munk function.

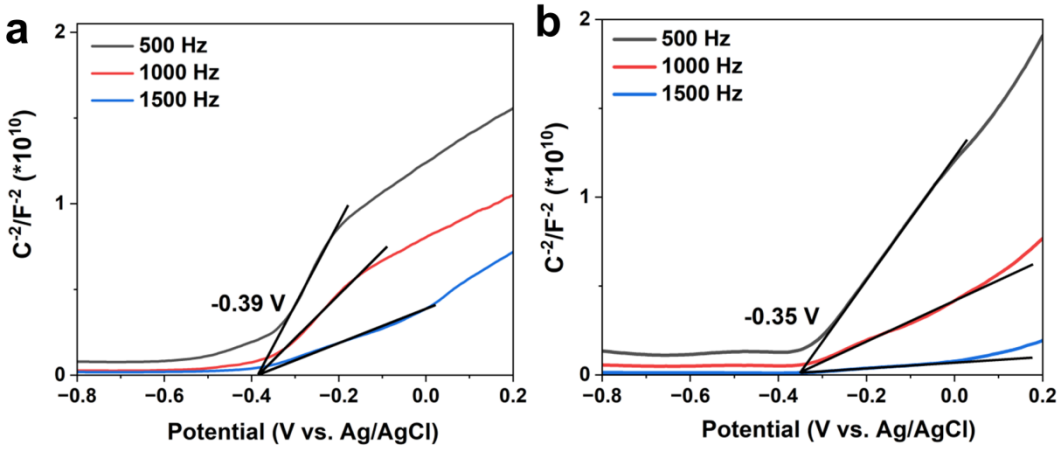

Fig S20. Mott-Schottky plots of (a) BOIO and (b) Rh_1/BOIO under different frequency. The flat band potential obtained by the M-S plots is approximately 0.1 V below their conductor band positions for n-type semiconductors.

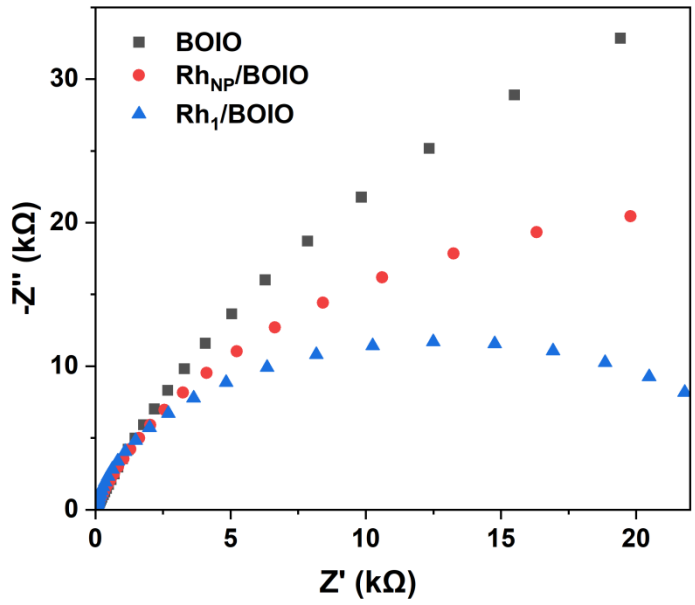

Fig S21. The EIS plots of samples.

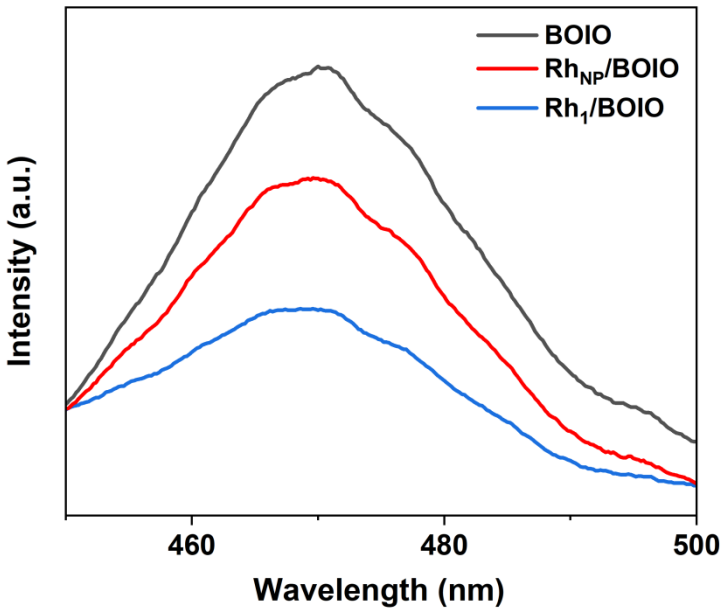

Fig S22. The steady-state PL spectra results of samples.

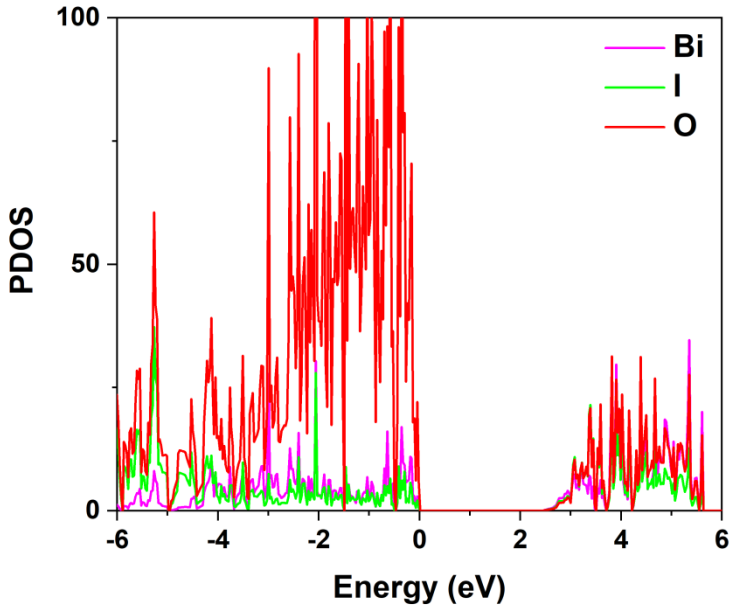

Fig S23. The PDOS results of BOIO.

Table S1. Structural parameters extracted from the Rh K-edge EXAFS fitting. (S_0^2=0.74)

Sample	Scattering pair	CN	R(Å)	$\sigma^2(10^{-3}Å^2)$	ΔE_0(eV)	R factor
Rh_1/BOIO	Rh-O	2.32	2.03	4.13	-0.51	0.009
Rh foil	Rh-Rh	12*	2.68	3.82	4.64	0.014

S_0^2, CN and R is the amplitude reduction factor, coordination number and interatomic distance (the bond length between central atoms and surrounding coordination atoms), respectively; σ^2 is Debye-Waller factor (a measure of thermal and static disorder in absorber-scatterer distances); ΔE_0 is edge-energy shift (the difference between the zero kinetic energy value of the sample and that of the theoretical model). R factor is used to value the goodness of the fitting.

* This value was fixed during EXAFS fitting, based on the known structure.

Error bounds that characterize the structural parameters obtained by EXAFS spectroscopy were estimated as N ± 10%; R ± 1%; σ^2 ± 15%; ΔE_0 ± 20%.

Rh_1/BOIO (FT range: 2.0-11.1 $Å^{-1}$; fitting range: 1.05-2.0 Å)
Rh foil (FT range: 3.0-14.0 $Å^{-1}$; fitting range: 1.0-2.8 Å)

Table S2. BA photo-oxidation performances over Rh_1/BOIO.

Photocatalyst	Product	Conversion (%)	Selectivity (%)	Reference
Rh_1/BOIO	BN	99.9	86.7	This work
RuO_2/Al_2O_3		75	49	1
Ru−K−ZrO_2		66	81	2
3%Ru/AC		99.9	81.7	3
[Ru(phen)(PPh_3)$_2$(CO)(H)]ClO_4		93	82	4
$RuCl_3$		100	53	5
Ru@E-MoS_2		19	99	6
[RuCl(bhq)(tpy)][PF_6]		74	—	7

Table S3. BA photo-oxidation performances over Rh_{NP}/BOIO.

Photocatalyst	Product	Conversion (%)	Selectivity (%)	Reference
Rh_{NP}/BOIO	N-BBA	99.9	82.8	This work
meso-MoOx-300		77	13	8
NH_2-MIL-125(Ti)/amorphous TiO_2		75	73	9
TiO_2		81	63	10
g-C_3N_4/BiOBr		63.1	87	11
WS_2		85	85	12
TiO_2 nano-flower-4h		99	73.3	13
UiO-66NH_2-@$Au_{0.5}$@COF1		66.9	96	14
WO_3/BiOBr		63.8	87	15
$BiOI_{0.2}Cl_{0.8}$		77.5	96	16
Cu catalysts		82.2	99	17

Table S4. The average lifetimes of different samples.

Samples	τ_1 (ns)	A_1	τ_2 (ns)	A_2	τ_{avg} (ns)
BOIO	0.8538	228.6940	6.8506	1.5270	1.1587
Rh_{NP}/BOIO	0.8642	218.7880	4.7132	4.0910	1.2204
Rh_1/BOIO	0.8817	205.5880	4.0689	7.6420	1.3484

References

1. Nordvang, E. C.; Schill, L.; Riisager, A.; Fehrmann, R. Ruthenium Dioxide Catalysts for the Selective Oxidation of Benzylamine to Benzonitrile: Investigating the Effect of Ruthenium Loading on Physical and Catalytic Properties. *Top. Catal.* **2017**, *60*, 1449−1461.
2. Zhu, G.; Shi, S.; Feng, X.; Zhao, L.; Wang, Y.; Cao, J.; Gao, J.; Xu, J. Switching Amine Oxidation from Imines to Nitriles by Carbon-Hydrogen Bond Activation via Strong Base Modified Strategy. *ACS Appl. Mater. Interfaces* **2022**, *14*, 52758−52765.
3. Niu, B.; Lu, F.; Zhang, H.-Y.; Zhang, Y.; Zhao, J. Synthesis of Nitriles from Aerobic Oxidation of Amines Catalyzed by Ruthenium Supported on Activated Carbon. *Chem. Lett*. **2017**, *46*, 330−333.
4. Ray, R.; Chandra, S.; Yadav, V.; Mondal, P.; Maiti, D.; Lahiri, G. K. Ligand controlled switchable selectivity in ruthenium catalyzed aerobic oxidation of primary amines. *Chem. Commun*. **2017**, *53*, 4006−4009.
5. Tang, R.; Diamond, S. E.; Neary, N.; Mares, F., Homogeneous catalytic oxidation of amines and secondary alcohols by molecular oxygen. *J. Chem. Soc., Chem. Commun*. **1978**, 562.
6. Asif Hussain, M.; Yang, M.; Jang, H.-S.; Hwang, S.-Y.; Um, B.-H.; Choi, B. G.; Kim, J. W. Two-Dimensional Heterogeneous Ruthenium−Molybdenum Disulfide Nanocatalyst for the Selective Aerobic Oxidation of Amines. *Ind. Eng. Chem. Res.* **2016**, *55*, 7043−7047.
7. Aiki, S.; Taketoshi, A.; Kuwabara, J.; Koizumi, T.-A.; Kanbara, T., The catalytic activity of a cyclometalated ruthenium(III) complex for aerobic oxidative dehydrogenation of benzylamines. *J. Organomet. Chem.* **2011**, *696*, 1301−1304.

8. Shubhashish, S.; Khanna, H. S.; Achola, L. A.; Amin, A. S.; Willis, W. S.; Suib, S. L. Selective Oxidative Coupling of Amines Using Mesoporous MoO_x Catalysts. *ACS Appl. Nano Mater.* **2021**, *4*, 2086−2097.
9. Sheng, W.; Huang, F.; Lang, X. NH_2-MIL-125(Ti)/amorphous TiO_2 microspheres for enhanced visible light photocatalytic selective oxidation of amines. *Mater. Today Chem.* **2023**, 30, 101505.
10. Li, N.; Lang, X.; Ma, W.; Ji, H.; Chen, C.; Zhao, J., Selective aerobic oxidation of amines to imines by TiO_2 photocatalysis in water. *Chem. Commun.* **2013**, *49*, 5034.
11. Juntrapirom, S.; Anuchai, S.; Thongsook, O.; Pornsuwan, S.; Meepowpan, P.; Thavornyutikarn, P.; Phanichphant, S.; Tantraviwat, D.; Inceesungvorn, B., Photocatalytic activity enhancement of g-C_3N_4/BiOBr in selective transformation of primary amines to imines and its reaction mechanism. *Chem. Eng. J.* **2020**, *394*, 124934.
12. Raza, F.; Park, J. H.; Lee, H.-R.; Kim, H.-I.; Jeon, S.-J.; Kim, J.-H. Visible-Light-Driven Oxidative Coupling Reactions of Amines by Photoactive WS_2 Nanosheets. *ACS Catal.* **2016**, *6*, 2754−2759.
13. Bu, J.; Fang, J.; Leow, W. R.; Zheng, K.; Chen, X. Single-crystalline rutile TiO_2 nano-flower hierarchical structures for enhanced photocatalytic selective oxidation from amine to imine. *RSC Adv.* **2015**, *5*, 103895−103900.
14. Zhang, K.; Xi, Z.; Wu, Z.; Lu, G.; Huang, X., Visible-Light-Induced Selective Oxidation of Amines into Imines over UiO-66-NH_2@Au@COF Core-Shell Photocatalysts. A*CS Sustainable Chemistry & Engineering* **2021**, *9*, 12623−12633.
15. Khampuanbut, A.; Santalelat, S.; Pankiew, A.; Channei, D.; Pornsuwan, S.; Faungnawakij, K.; Phanichphant, S.; Inceesungvorn, B. Visible-light-driven WO_3/BiOBr heterojunction photocatalysts for oxidative coupling of amines to imines: Energy band alignment and mechanistic insight. *J. Colloid Interface Sci.* **2020**, *560*, 213−224.
16. Anuchai, S.; Tantraviwat, D.; Nattestad, A.; Chen, J.; Inceesungvorn, B., Tuning product selectivity and visible-light-driven activity in oxidative coupling of amines to imines: A case study of $BiOI_xCl_{1-x}$ photocatalyst. *Colloids and Surfaces A: Physicochemical and Engineering Aspects* **2021**, *629*, 127481.
17. Chai, Y.; Zhang, L.; Liu, Q.; Yang, F.; Dai, W.-L. Insights into the Relationship of the Heterojunction Structure and Excellent Activity: Photo-Oxidative Coupling of Benzylamine on CeO_2-rod/g-C_3N_4 Hybrid under Mild Reaction Conditions. *ACS. Sustain. Chem. Eng.* **2018**, *6*, 10526−10535.